Impacts of tropical cyclone-heatwave compound events on surface ozone in eastern China: Comparison between the Yangtze River and Pearl River Deltas

Cuini Qi [1], Pinya Wang [1, *], Yang Yang [1, *], Huimin Li [1], Hui Zhang [1], Lili Ren [2], Xipeng Jin [1], Chenchao Zhan [3], Jianping Tang [4], Hong Liao [1]

[1]Jiangsu Key Laboratory of Atmospheric Environment Monitoring and Pollution Control, Jiangsu Collaborative Innovation Center of Atmospheric Environment and Equipment Technology, Joint International Research Laboratory of Climate and Environment Change, School of Environmental Science and Engineering, Nanjing University of Information Science and Technology, Nanjing, Jiangsu, China

[2]College of Environment and Ecology, Jiangsu Open University, Nanjing, Jiangsu, China

[3]School of Atmospheric Physics, Nanjing University of Information Science and Technology, Nanjing, Jiangsu, China

[4]School of Atmospheric Sciences, Nanjing University, Nanjing, Jiangsu, China

Correspondence to: Pinya Wang, pinya.wang@nuist.edu.cn

Yang Yang, yang.yang@nuist.edu.cn

Abstract

China has implemented some air pollution management measures in recent years, yet severe ozone pollution remains a significant issue. The Southeastern Coast of China (SECC) is often influenced by hot extremes and tropical cyclones (TCs), and the two can occur simultaneously (TC-HDs). The compound TC-HDs show a rising trend in the summers of 2014-2019, potentially affecting ozone pollution. Here, we found that surface ozone concentrations over SECC are more elevated during extreme hot days than the summer climatology. However, compared to extreme hot days alone (AHDs), the maximum 8-hour average ozone (MDA8 O_3) concentration increases by an average of 6.8 $\mu g/m^3$ in the Pearl River Delta (PRD) and decreases by 13.2 $\mu g/m^3$ in the Yangtze River Delta (YRD) during the compound TC-HDs. The meteorological conditions during AHDs favor the chemical production of ozone over SECC, exhibiting increased temperature and solar radiation but decreased relative humidity. Relative to AHDs, strong northeasterly winds prevail in SECC during TC-HDs, suggesting the potential of ozone cross-regional transport between YRD and PRD. The process analysis in the chemical transport model (GEOS-Chem) suggests that relative to AHDs, the chemical production of ozone is enhanced in YRD during TC-HDs while horizontal transport alleviates ozone pollution in YRD but worsens it in PRD through cross-regional transport. The results highlight the significant effects of cross-regional transport in modulating ozone pollution in the two megacity clusters during hot extremes accompanied by TC activities, giving insight into future ozone control measures over SECC under global warming.

1. Introduction

Tropospheric ozone (O_3) is the predominant air pollutant in addition to fine particulate matter ($PM_{2.5}$) in China (Fu et al., 2019), and it poses significant risks to human health and the ecosystem (Feng et al., 2015; T. Wang et al., 2017). Long-term exposure to high concentrations of ozone could lead to lung tissue damage and chronic obstructive pulmonary disease, thereby increasing premature death (Turner et al., 2016; Liu et al., 2018). Chen et al. (2023) demonstrated that the deterioration of ozone air quality is considered to be the primary factor responsible for the 90% increase in premature respiratory mortalities in China from 2013 to 2019. Furthermore, ozone can negatively impact crop yield by inhibiting plant photosynthesis, accelerating crop senescence, and reducing both yield and quality (Ainsworth et al., 2012; Song and Hao, 2023), ultimately affecting ecosystem stability (Gu et al., 2023).

To deal with the severe air pollution issues, China has implemented several pollution prevention and control measures, which are prioritized to tackle the problem of particulate matter (P. Wang et al., 2022), including the "Air Pollution Prevention and Control Action Plan" and the "Three-Year Action Plan for Winning the Blue Sky Defense Battle". As a result, these efforts are making significant progress in lowering $PM_{2.5}$ concentrations. Z. Wang et al. (2022) indicated that the annual concentration of $PM_{2.5}$ in China has decreased by 13.41 $\mu g/m^3$ from 2014 to 2020. However, it is worth noting that most cities in China still frequently experienced severe ozone episodes (K. Li et al., 2019). It is demonstrated that surface ozone concentration in most regions of China have increased by approximately 20% during the period from 2013 to 2017 (Huang et al., 2018). Also, Wei et al. (2022) recently found that both surface ozone concentration and ozone

pollution (the maximum 8-hour average ozone (MDA8 O_3) concentrations exceed 160 $\mu g/m^3$) days in China exhibited an increasing trend from 2013 to 2020. Therefore, ozone pollution in China has received widespread attention over the past few decades (Ashmore, 2005; Gong and Liao, 2019; N. Wang et al., 2022).

Changes in tropospheric ozone are closely related to their precursor gases, including nitrogen oxides (NO_x) and volatile organic compounds (VOCs) (Fu and Liao, 2014; Jacob et al., 1999; K. Li et al., 2019). Zhang et al. (2023) revealed that an increase in biogenic volatile organic compounds (BVOCs) increased local ozone production by 23% per year in Hong Kong. K. Li et al. (2019) pointed out that anthropogenic NOx emissions in China decreased by 21% from 2013 to 2017, whereas VOCs emissions changed little. Decreasing NOx would increase ozone under the VOC-limited conditions prevailed in urban China but decrease ozone under rural NO_x-limited conditions. In addition to precursor emissions, meteorological conditions can significantly modulate surface ozone levels (Yin et al., 2019; Zhou et al., 2022). For example, severe ozone pollution commonly occurs during summertime with high temperatures, low relative humidity (RH), and strong solar radiation (Dai et al., 2023; Yin et al., 2019). Under low RH conditions, trees close the stomata (pores for exchanging CO_2 and water vapor), inhibiting the dry deposition of ozone and leading to ozone accumulation (Kavassalis and Murphy, 2017). Besides, low humidity conditions inhibit ozone breakdown as the $O(^1D)$ combines with water molecules (H_2O) to produce hydroxyl radicals that promote ozone decomposition in high humidity environments (M. Li et al., 2021). Wind direction and wind speed play an important role in the transport and diffusion of ozone (Banta et al., 2011; Jammalamadaka and Lund, 2006). It is proved that the co-occurred heat waves and atmospheric

82 stagnation days with low wind speed favor ozone pollution in the U.S. through promoting the ozone
83 production (Zhang et al., 2018). Reduced clouds and strengthened solar radiation during the hot
84 extremes favor photochemical ozone production in the troposphere and thus increase the surface
85 ozone concentrations (P. Wang et al., 2022). Large-scale atmospheric circulation can modulate
86 surface ozone through changing the meteorological conditions (Yang et al., 2022). For instance, the
87 stronger western Pacific subtropical high (WPSH) leads to higher temperatures, stronger solar
88 radiation, lower RH, and less precipitation, which favors the production and accumulation of surface
89 ozone in northern China (Jiang et al., 2021).

90 Extreme weather events, especially heat waves and tropical cyclones (TCs), have a significant
91 impact on ozone in eastern China (Lin et al., 2019; T. Wang et al., 2017). High ozone concentration
92 events are typically associated with high temperatures, which lead to increased emissions of BVOCs
93 and enhance the chemical formation of ozone (Lu et al., 2019; P. Wang et al., 2022). TC activities
94 can substantially affect tropospheric ozone through affecting the transport, production and
95 accumulation processes over the coastal regions of China (K. Meng et al., 2022; Qu et al., 2021;
96 Zhan et al., 2022). For ozone pollution over the Yangtze River Delta (YRD) region, the peripheral
97 circulations of approaching TCs intensify downward airflow, resulting in a short-term local weather
98 pattern of high temperatures, low humidity, intense solar radiation, and light winds, exacerbating
99 ozone pollution (Shu et al., 2016). Following the passage of TCs, the lower tropospheric transport
100 of ozone-rich air and strong photochemical reactions also contribute to amplifying ozone pollution
101 (Zhan et al., 2020). For ozone pollution in Pearl River Delta (PRD), influenced by the strong
102 downdrafts related to the periphery of TCs, the PRD region typically is dominated by high pressure,

low humidity, and strong solar radiation, leading to the accumulation of ozone (Wei et al., 2016; Ouyang et al., 2022). Moreover, TC activities are proven to enhance the chemical interactions between anthropogenic and biogenic emissions, resulting in extreme ozone pollution over both the YRD and PRD regions (N. Wang et al., 2022).

The southeastern coastal region of China (SECC), including the YRD and PRD regions, experiences both frequent TCs and heatwave events under global warming (W. Wang et al., 2016; Xiao et al., 2011). And there is a significant concurrent relationship between extreme heatwaves and TC activity that the peripheral circulations of TCs can promote extreme heatwaves (P. Wang et al., 2023; Zhang et al., 2024). Such compound hazards are more destructive than the individual extremes (Matthews et al., 2019). The SECC region has experienced a considerable rise in surface ozone concentrations during the period from 2013 to 2019 (X. Meng et al., 2022). Although the individual effects of heatwaves and TCs on ozone have been emphasized, the effects of the compound extremes of heat waves and TCs on ozone pollution have received limited attention.

In this study, we aim to investigate the impacts of the compound hazards of TCs and extreme hot days (TC-HDs) on ozone pollution in SECC (105-125° E,10-35° N) based on the long-term (2014-2019) observational records of air temperatures and TCs, reanalysis datasets of ground-level ozone concentrations and meteorological parameters, and the GEOS-Chem model simulations. The mechanisms contributing to these impacts are also analyzed. The study is organized as follows: Section 2 presents the methods and data utilized, and Section 3 describes the spatial and temporal variations of TC-HDs observed in SECC during 2014-2019. Section 4 describes the impacts of TC-HDs on ozone concentration in SECC, with a focus on YRD and PRD regions. In Section 5, we

investigate the possible mechanisms for the anomalous ozone concentrations in SECC during TC-HDs as well as the differences between YRD and PRD by investigating the meteorological conditions and key chemical and physical process analysis with the GEOS-Chem model. Finally, Section 6 provides a summary and discussion.

2. Data and methods

2.1 Observational datasets

In this work, we focus on the ozone pollution over SECC where is vulnerable to both severe hot extremes and ozone pollution (Ma et al., 2019; P. Wang et al., 2022). A topographic map of the SECC including the YRD and PRD regions is shown in Figure 1. The daily maximum air temperatures (Tmax) from more than 1400 observation sites in the domain for the period 2014-2019 are provided by the China Meteorological Administration (CMA). The best track dataset of TCs is also released by CMA (accessible at https:// tcdata.typhoon.org.cn/zjljsjj_sm.html). This dataset includes the time, location, and intensity of TCs, which records all TCs that have passed through the western North Pacific (WNP) since 1949 (Lu et al., 2021; Ying et al., 2014).

2.2 Reanalysis datasets

The ground-level ozone concentrations for the period 2014-2019 are obtained from the high-resolution and high-quality ground-level MDA8 ozone data (unit: $\mu g/m^3$) for China (ChinaHighO_3) at a resolution of 0.1° × 0.1°, which is one of the series of the high-resolution and high-quality ground-level air pollutants in China (Wei et al., 2022). The ChinaHighO_3 dataset provides reliable estimates of MDA8 ozone, demonstrated by an average out-of-sample (out-of-station) coefficient of determination of 0.87 (0.80) and a root-mean-square error of 17.10 (21.10) $\mu g/m^3$ across China

(Wei et al., 2022).

Meteorological parameters including 2-meter air temperature (T2m), relative humidity (RH), surface solar radiation downwards (SSRD), geopotential height (HGT), eastward wind (uwnd), northward wind (vwnd), mean sea level pressure (MSLP), total cloud cover (TCC), vertical integral of eastward water vapour flux, vertical integral of northward water vapour flux and vertically integrated moisture divergence are from the fifth generation of the European Centre for Medium-Range Weather Forecasts (ECMWF) reanalysis data (ERA5), the latest global atmospheric reanalysis of ECMWF (Hersbach et al., 2020). The temporal resolution for T2m, SSRD, and TCC is 6 hours, while that for other meteorological parameters is 3 hours, which are all utilized to generate daily mean values.

2.3 Identifications of extreme events

Severe ozone pollution episodes generally occur in SECC during summertime, coinciding with frequent heatwaves and TCs (Ji et al., et al., 2024; Shu et al., 2016). In this work, we focus on the impacts of extreme high temperatures and TCs on surface ozone during summer only (June, July, and August) in SECC, as outlined in Figure 1. P. Wang et al. (2022) pointed out that most TC tracks over the western North Pacific passed through the SECC region during their lifetimes in the past several decades. The hot days (HDs) are defined as dates when the number of high-temperature sites (Tmax≥35℃) exceeds more than 40% of the total number of observation stations within the SECC. We use the proportion of high-temperature sites exceeding 40% as a measure of HDs to ensure adequate samples and extremely hot conditions over SECC during HDs. Note that the anomalies of surface ozone concentrations exhibit consistent spatial patterns during HDs identified by with a

lower (30%) or higher (50%) criterion for the percentage of high-temperature sites (figures not shown). In this work, we classify all HDs into two categories: tropical cyclone-hot days (TC-HDs) and alone hot days (AHDs). TC-HDs are identified when hot days occur over the land regions within SECC, concurrent with the passages of tropical cyclones through the area; and AHDs indicate hot days that occur independently.

In this work, the least squares method is applied to fit the linear trend and the Student' s t-test is used to test the significance of the trend ($\alpha = 0.05$). A p-value < 0.05 indicates the statistically significant trend (as shown in Figure 2). The Student's t-test is also used to evaluate the significance of the differences in ozone concentrations and meteorological variables between HD/TC-HDs and the long-term climatology.

2.4 GEOS-Chem model

In this study, surface ozone concentrations during 2014-2019 are simulated by using the 3-D global chemical transport model (GEOS-Chem, version 13.4.1) with a horizontal resolution of 2° latitude × 2.5° longitude and 47 vertical layers from the surface to 0.01 hPa. The GEOS-Chem has the fully coupled O_3–NO_x–hydrocarbon–aerosol chemical mechanisms (Pye et al., 2009; Sherwen et al., 2016) used to simulate concentrations of gas-phase pollutants (such as ozone) and aerosols. It is driven by assimilated meteorological data of version 2 of Modern-Era Retrospective analysis for Research and Applications (MERRA2; Gelaro et al., 2017)

The anthropogenic emissions of ozone precursor gases, including CO, NOx, and non-methane volatile organic compounds (NMVOCs) are provided by the Community Emissions Data System (CEDS) (Hoesly et al., 2018). Methane (CH_4) concentrations are provided by the Global Monitoring

187 Division (GMD) of the National Oceanic and Atmospheric Administration (NOAA). Biomass
188 burning emissions are obtained from the Global Fire Emissions Database version 4 (GFEDv4) (Van
189 Der Werf et al., 2017). The biogenic emissions are estimated with the Model of Emissions of Gases
190 and Aerosols from Nature (MEGAN) version 2.1(Guenther et al., 2012). Our previous studies show
191 that GEOS-Chem model excels in accurately reproducing observed ozone concentrations and spatial
192 distributions in China (Yang et al., 2022, 2014).

193 Meteorological conditions can modulate surface ozone concentrations through affecting the
194 physical and chemical processes including chemical production, horizontal advection, vertical
195 advection, dry deposition and diffusion (Gong and Liao, 2019). In this work, we quantify the
196 contributions of individual processes to ozone changes using the model outputs of GEOS-Chem
197 (Gong and Liao, 2019; Ni et al., 2024; Shu et al., 2016). In the GEOS-Chem model, the change in
198 ozone over time step are caused by chemical production, horizontal advection, vertical advection,
199 dry deposition and diffusion, which can be used for separating out and quantifying the contributions
200 of individual physical and chemical processes to the changes in the simulated ozone concentrations
201 (Gong and Liao, 2019; Ni et al., 2024; Shu et al., 2016).

202 **3. Spatial and temporal variations of compound TC-HDs**

203 There are 63 days of TC-HDs over SECC during the summers of 2014-2019, accounting for
204 around 70% of the total HDs (91 days), with 28 hot days (30%) occurring alone (AHDs) in the past
205 6 years. The monthly variations of HDs, TCs, and TC-HDs over SECC from 2014 to 2019 are
206 displayed in Figure 2. All the weather extremes show notable intraseasonal variations with relatively
207 higher occurrences in July and August but lower occurrences in June each year. Besides, both the

occurrences of HDs and TCs demonstrate significant upward trends at the 90% confidence level, with a rate of 0.31 days per month and 0.33 days per month, respectively. TC-HDs also show an increasing trend with a rate of increase of 0.2 days/month, consistent with the variations of HDs and TCs in the past six years. Hence, it is essential to examine the effects of rising TC-HDs on ozone pollution in the SECC region.

Figure 3 demonstrates the spatial features of TC-HDs during 2014-2019. China Meteorological Administration classifies tropical cyclones into 6 classes based on their intensity, namely Tropical Depression (TD, 10.8-17.1 m/s), Tropical Storm (TS, 17.2-24.4 m/s), Strong Tropical Storm (STS, 24.5-32.6 m/s), Typhoon (TY, 32.7-41.4 m/s), Strong Typhoon (STY, 41.5-50.9 m/s) and Super Typhoon (SSTY, ≥51.0 m/s). TCs are generally stronger before their landfalls, which can reach STY and even SSTY (Fig. 3a and 3b), consistent with previous findings (Han et al., 2022; Tuleya et al., 1984). TCs that affect the SECC primarily originate east of 135° E and move westward to the eastern coastal regions. Around 90% of TCs associated with TC-HDs make landfalls while the others weaken and dissipate over the ocean. Moreover, the air temperatures over land regions of SECC during the TC-HDs are generally high, where the average Tmax of most sites are beyond 35℃ and reach up to 38℃ (Fig. 3a). Compared with the summer climatology from 2014 to 2019, the average Tmax during TC-HDs increased approximately 4℃ over most land regions of SECC (Fig. 3b).

The temporal variations of the proportion of high-temperature sites (Tmax≥ 35℃) and the temperature anomalies relative to the summertime climatology averaged for the SECC land regions along with the movements of TCs are given in Figs. 3c and 3d. Specifically, in Figures 3c&3d, the

229 colored dots along the movements of TC tracks represents the proportion of high-temperature sites
230 and the average temperature anomalies relative to the summertime climatology in SECC at that time,
231 respectively. The two variables demonstrate similar patterns of variation. As TCs approach land
232 regions, both the high-temperature sites and temperature anomalies are increasing gradually, with a
233 particularly pronounced temperature increase associated with TCs moving towards the PRD regions.
234 In contrast, there is typically a decline in both the average air temperatures and the proportion of
235 high-temperature sites following the landfalls of TCs, which could be related to the strong wind and
236 rainfall associated with the TCs (Gori et al., 2022).

237 **4. Influences of TC-HDs on surface ozone concentrations in SECC**

238 Extreme high temperatures and the accompanied meteorology such as high-pressure systems
239 and strong radiation can affect local ozone pollution by enhancing chemical production and/or
240 accumulation (Gong and Liao, 2019; P. Wang et al., 2022; X. Wang et al., 2009). It is also well
241 demonstrated that extreme high temperatures and TCs can affect the ozone pollution over coastal
242 regions of China (Ding et al., 2023; Huang et al., 2011; N. Wang et al., 2022). In this work, we
243 further focus on the impacts of TC-HDs on surface ozone concentrations over land regions of SECC.
244 Figure 4 presents the spatial distributions of ozone concentration anomalies during TC-HDs and
245 AHDs relative to the summertime climatology from 2014-2019, as well as the differences between
246 the two. Notable increases in surface ozone concentrations are observed over most land regions of
247 SECC during the AHDs period, with anomalous MDA8 ozone reaching 40 $\mu g/m^3$ and 20 $\mu g/m^3$
248 over the YRD (118-122° E, 30-33° N) and PRD (110-115.5° E, 21.5-24° N) regions, respectively
249 (Fig. 4a), consistent with previous finding that hot extremes can worsen ozone pollution (P. Wang

et al., 2022). During the compound TC-HDs, most land regions except Hainan Island and the northern part to 33° N of SECC experience a significant enhancement in surface ozone concentrations, with MDA8 ozone anomalies above 20 μg/m^3 overall (Fig. 4b). Compared to AHDs, ozone concentrations in the easternmost coastal regions of China including YRD (outlined in Fig. 4c) are suppressed while ozone concentrations over the southernmost coastal regions of China including PRD (outlined in Fig. 4c) are promoted during the compound TC-HDs. Comparing to TCs occurring alone, surface ozone concentrations over most land regions of SECC increase during TC-HDs (Fig. S1), which should be attributed to the increases in air temperatures. In this work, we deliberately investigate the enhanced surface ozone concentration of PRD and the contrasting depression over YRD during the compound TC-HDs.

The temporal variations of anomalous MDA8 ozone in YRD and PRD regions relative to the summertime climatology with TC tracks during TC-HDs are shown in Figure 5. In Figures 5a&5b, the colored dots along the TCs track represents the anomalies of regional mean MDA8 ozone concentrations for YRD and PRD at that time compared with the summertime climatology for 2014-2019. Surface ozone concentrations over YRD are abnormally higher when TCs are positioned a long distance from land regions, whereas ozone concentrations fall dramatically when TCs approach and make landfall over land regions. And it should be noted that the surface ozone concentrations are elevated by the TCs moving westward YRD while most of the other TCs cause a decline in ozone concentrations with their approach to land regions, consistent with previous work (Shu et al., 2016). Zhan et al. (2020) revealed that O_3 pollution episodes in YRD mainly occurred near the 24-hour warning line before a TC landed on the coastline. The region was impacted by an inland wind

carrying substantial precursor substances from polluted areas, while approaching TCs led to increased precipitation and strong winds resulting in decreased ozone concentrations. For PRD, surface ozone concentrations increase noticeably when TCs approaching land regions. Particularly, the TCs heading northeast to YRD favor the increases in ozone concentrations in the PRD whereas the others tend to cause a reduction in surface ozone concentrations following landfalls.

5. Possible mechanisms underlying the impacts of TC-HDs on surface ozone

5.1 The dominant synoptic circulations

The synoptic meteorological conditions during AHDs and TC-HDs are analyzed to disentangle the different responses of surface ozone to hot extremes superimposed by TCs. Specifically, we examine the composites of daily mean air temperature at 2m (T2m), relative humidity (RH), surface solar radiation downwards (SSRD), mean sea level surface (MSLP), geopotential height at 500 hPa (500hPa HGT) and 10-meter wind speeds, and total cloud cover (TCC) anomalies relative to summertime climatology from 2014 to 2019 during AHDs (Fig. 6) and TC-HDs (Fig. 7), as well as the differences between the two periods (Fig. 8). During the AHDs period, the land regions of SECC are covered by increased T2m, decreased RH, reduced TCC, and enhanced SSRD (Figs. 6a-d), which are favorable for the chemical formation of ozone therein (Yin et al., 2019), supporting the elevated surface ozone during AHDs as shown in Figure 4a. In the mid-upper troposphere, a band of positive HGT at 500hPa (H500) anomalies predominates over most land regions of China, extending northeastward to Korea (Fig. 6e). This pattern features westerly wind anomalies in the northern flank and easterly wind anomalies in the southern flank, indicating a westward extension and strengthening of the western North Pacific subtropical high (WNPSH). These conditions favor

292 the occurrences of hot extremes over southern China, as discussed by Luo & Lau (2017) and P.
293 Wang et al. (2018). Besides, it's noticed that negative H500 anomalies and cyclonic circulation
294 appear over the east of 125° E which are also seen at the surface (Fig. 6f) with anomalous
295 southwesterly prevails over SECC land regions at the surface (Fig. 6f). Such a low-pressure system
296 characterizes TC track which finally recurve northeastward (Fig. S2).

297 During TC-HDs, the most land regions of SECC are covered by increased T2m, decreased RH,
298 reduced TCC, and enhanced SSRD (Figs. 7a-d), favoring the enhanced chemical formation of ozone
299 therein, supporting the elevated surface ozone during TC-HDs as shown in Figure 4b. In the mid-
300 upper troposphere, positive H500 anomalies cover nearly the whole land region of China with
301 maximum dominating Korea, accompanied by anomalous anticyclonic circulation. Such changes
302 characterize the strengthening and westward extension of WPSH (Fig. 7e), favoring more hot
303 extremes. A dipole pattern of MSLP anomalies can be observed at the surface, with an abnormal
304 low-pressure center over the South China Sea and another to its east (Fig. 7f). Besides, the land
305 regions are influenced by weak winds at the surface (Fig. 7f). Particularly, for the decrease MDA8
306 ozone, we can see that during TC-HDs, Hainan islands is covered by decreased T2m, increased RH,
307 reduced SSRD, and increased TCC (Figs. 7a-d), along with negative H500 and MSLP anomalies
308 (Figs. 7e&f). Such meteorological conditions in Hainan islands may suppress the chemical
309 production of ozone and the oceanic winds may clean the air (Fig. 7e). On the other hand, for the
310 north part of SECC, the circulation anomalies favor strengthened southeastern moisture flow and
311 enhance the convergence of water vapor flux there (Fig. S3), which can lead to increased relative
312 humidity (Fig.7b). The local higher temperature (Fig. 7a) and humid conditions may favor

convection activities (P. Wang et al., 2019b), characterized increased cloud cover (Fig. 7d) and decreased surface solar radiation (Fig. 7c). These meteorological conditions can inhibit the local ozone production and cause a lower ozone concentration in north part of the SECC during TC-HDs.

Figure 8 demonstrates the differences in meteorological variables between the periods of TC-HDs and AHDs. Compared to AHDs, the YRD experiences an increase in T2m of approximately 1℃, while the PRD experiences a decrease in T2m of around 0.5℃ during TC-HDs. In the meanwhile, RH and TCC values are increased (decreased) in PRD (YRD) while SSRD values are decreased (increased) in PRD (YRD) (Figs. 8a-d). The large-scale circulations in the middle-upper troposphere show positive H500 anomalies over the north and northeast parts of China including YRD while southern China including PRD is dominated by negative H500 anomalies, supporting the increased T2m (decreased) over YRD (PRD). Moreover, a cyclonic circulation controls southern China with YRD influenced by strong southeasterly winds while PRD is influenced by inland northeasterly winds (Fig. 8e). The changes in MSLP show a similar pattern to H500 anomalies with positive anomalies over YRD but negative anomalies over PRD, and an anomalous low-pressure system is observed over South China Sea, accompanied by strong cyclonic circulation at the surface. It should be noted that the YRD is influenced by strong easterly winds from the ocean and the clean winds may alleviate ozone pollution as shown in Figure 4c. In contrast, PRD is influenced by strong northeasterly winds from inland which is opposite to the climatological southwesterlies of the summer monsoon circulation, which may favor the accumulation of ozone pollution therein, as shown in Fig. 4c

It should be noted that the mereological conditions in YRD favor the chemical production of

ozone yet reduced ozone concentrations are observed in YRD during TC-HDs relative to AHDs. The key physiochemical processes associated with the alleviated ozone pollution over YRD but worsened ozone pollution over RPD during TC-HDs relative to AHDs are explored with GEOS-Chem model simulations in the following part.

5.2 Process analysis with GEOS-Chem model simulations

In this section, process analysis is conducted in the GEOS-Chem model to quantify the contributions of each process, including net chemical production, horizontal advection, vertical advection, and mixing (diffusion and dry deposition) to the anomalous surface ozone concentrations over PRD and YRD during TC-HDs, respectively. The observed and simulated anomalous surface MDA8 ozone during TC-HDs relative to the summer climatology mean and AHDs are given in Figure S4 and the regional averages of surface MDA8 ozone concentrations over YRD and PRD are summarized in Table 1. GEOS-Chem simulation can reasonably capture the spatial pattern of anomalous surface MDA8 ozone concentrations during TC-HDs relative to the summer climatology mean (Figs. S4a and b), and relative to AHDs (Figs. S4c and d). Particularly, compared to AHDs, the simulated surface MDA8 ozone concentrations are inhibited over YRD but enhanced over PRD during TC-HDs. As listed in Table 1, compared to AHDs, during TC-HDs, the observed (simulated) average surface MDA8 ozone concentrations in the YRD decreased by 13.21 $\mu g/m^3$ (21.94 $\mu g/m^3$), whereas it increased by 6.8 $\mu g/m^3$ (7 $\mu g/m^3$) in the PRD. This suggests that the model simulation can reasonably capture the opposite changes in surface MDA8 ozone concentrations over the YRD and PRD during extreme HDs superimposed by TCs.

Figure 9 illustrates the vertical profiles of simulated daily mean ozone concentrations for YRD

and PRD from surface to 500 hPa for the summer climatology, TC-HDs and AHDs during 2014-2019, respectively. For YRD, surface ozone concentrations are apparently higher during AHDs than those during TC-HDs and summertime climatology from surface up to the 500 hPa level (Fig. 9a). This indicates that the enhancements in ozone concentrations during AHDs occur not only at the surface but also to the middle of the troposphere. In addition, compared with the summertime climatology, ozone concentrations in YRD during TC-HDs are slightly enhanced from surface to 850 hPa as well as between 600 hPa and 500 hPa while suppressed between 850hPa and 600 hPa. For the PRD, ozone concentrations during TC-HDs are higher than the summertime mean and AHDs from the surface up to 500 hPa (Fig. 9b). The ozone concentrations during AHDs are comparable to (slightly stronger than) the summertime mean below (above) 850 hPa (Fig. 9b) based on the GEOS-Chem model simulation.

We further analyze the main physiochemical processes affecting ozone concentration, including net chemical production, vertical advection, horizontal advection and mixing (the sum of dry deposition and diffusion). Figures 10 and 11 show the vertical profiles of the anomaly of each process during TC-HDs and AHDs, relative to the summertime climatology over the YRD and PRD, as well as the differences between TC-HDs and AHDs. During AHDs, the increase in ozone concentrations in the YRD from the surface to 900 hPa is primarily contributed by chemical production, while transport processes tend to decrease ozone concentration. Between 900 hPa and 700 hPa, the mixing process contributes to the increases in ozone concentrations while the transport processes and chemical productions tend to decrease ozone concentrations. Between 700 hPa and 500 hPa, horizontal transport hampers ozone increase, while chemical production and vertical

transport contribute to ozone enhancement (Fig. 10a). During TC-HDs, the horizontal transport exhibits a suppressive effect on ozone concentrations in the YRD from the surface up to 500 hPa whereas the chemical production contributes to increases in ozone concentration. And two processes overtake the effects of vertical transport and mixing (Fig. 10b). In comparison with AHDs, during TC-HDs, ozone concentration increases due to chemical production exceed decreases caused by horizontal transport between the surface and 850 hPa. However, between 850 hPa and 700 hPa, the decrease in ozone concentration due to horizontal transport outweighs the increase from chemical production. Overall, compared to AHDs, the chemical production contributes to increased ozone concentrations in the YRD from the surface up to 500 hPa during TC-HDs, whereas the horizontal transport tends to lower ozone concentrations. The relatively small differences in physicochemical processes between AHDs and TC-HDs around 700 hPa in the vertical profile are due to the minor effects of these processes during both AHDs and TC-HDs (not shown). As listed in Table 2, compared to AHDs, ozone chemical production plays a predominant role in enhancing ozone pollution during TC-HDs in the YRD (1.24 Gg O_3/day), whereas horizontal transport significantly depresses ozone concentration (−1.15 Gg O_3/day). As stressed above, the strong and clean oceanic winds along YRD can help alleviate ozone pollution. The vertical transport and mixing processes play a less important role in affecting ozone concentrations in YRD during TC-HDs.

For PRD, the horizontal transport primarily contributes to decreased ozone concentrations in the PRD between the surface and 500 hPa during AHDs. The chemical production, vertical transport and mixing processes exhibit promoting effects on ozone concentrations from surface to 700 hPa (Fig. 11a). During TC-HDs, horizontal transport predominantly contributes to increased ozone

concentrations over PRD from surface to 900 hPa and between 850 hPa and 500 hPa and the chemical production increases ozone concentrations between 950 hPa and 800 hPa. In contrast, the mixing process and vertical transport play a dominant role in reducing ozone concentrations between the surface to 900 hPa and between 900 hPa to 500 hPa respectively (Fig. 11b). Compared to AHDs, during TC-HDs, transport processes predominantly contribute to the increases in ozone concentrations in the PRD from the surface up to 500 hPa. Additionally, between 900 hPa and 800 hPa, chemical production plays a positive role in enhancing ozone concentrations. As listed in Table 3, during TC-HDs compared to AHDs, the horizontal transport process in the PRD exhibits a significantly stronger enhancing effect on ozone concentrations from surface to 500 hPa (1.81 Gg O_3/day) compared to the other three processes. Note that the summer climatology of ozone concentrations in YRD is significantly higher than that in PRD (Fig. S5) and the cross-section of wind anomalies demonstrates that strong winds from YRD to PRD exist during TC-HDs (Fig. S6), implying strong ozone mass transport from YRD to PRD. Thus, the cross-region transport may play a significant role in worsening ozone pollution over RPD during TC-HDs relative to AHDs.

In summary, favorable synoptic patterns during extreme hot days promote the chemical production of ozone, and thus exacerbate ozone pollution over both YRD and PRD. Compared to AHDs, the anomalously meteorological conditions during TC-HDs, enhance the chemical production of ozone in the YRD while the horizontal transport process mitigates ozone pollution therein but worsens ozone pollution in PRD though cross-regional transport, finally resulting in an increase in ozone in PRD but a decrease in YRD.

6. Conclusion and discussions

418 China has implemented a series of emission reduction strategies to alleviate air pollution, and
419 $PM_{2.5}$ concentrations have decreased significantly while ozone pollution remains a major concern.
420 Ozone pollution is sensitive to meteorological conditions, especially the extreme weathers that
421 frequently strike China under global warming. Eastern China is economically developed and
422 densely populated, with serious ozone pollution. It is also vulnerable to both extreme hot weathers
423 and TCs during the summer. In this work, we deliberately investigate the impacts of extreme hot
424 weathers on surface ozone for the summers of 2014-2019 over SECC coupled with (TC-HDs) and
425 without TCs (AHDs) over the ocean. The associated synoptic conditions and physicochemical
426 processes are assessed combined reanalysis dataset with the GEOS-Chem model simulations.
427 Results show that the surface ozone concentrations over most land regions within SECC are
428 elevated during both TC-HDs and AHDs relative to the climatological mean, however, there are
429 considerable differences between the two events. Relative to AHDs, the surface ozone
430 concentrations are noticeably decreased in the YRD region but increased in the PRD region during
431 TC-HDs periods. The meteorological conditions suggest that though YRD is influenced by higher
432 temperature, lower humidity, and stronger radiation during TC-HDs than AHDs, it is influenced by
433 strong and clean sea winds, which aid in ozone elimination. In contrast, the PRD is influenced by
434 the strong northeasterly winds, opposite to the climatology, and may transport ozone pollution from
435 polluted regions. Such a hypothesis is validated with the GEOS-Chem simulation. Compared with
436 AHDs, among all the physicochemical processes, horizontal transport plays a crucial role in
437 increasing (reducing) ozone levels over PRD (YRD). Compared to AHDs, the horizontal transport
438 contributes to -1.15 Gg O_3/day and 1.8 Gg O_3/day to the net changes in tropospheric ozone mass

from surface to 500 hPa in YRD and PRD during TC-HDs. The findings will provide significant implications for the control measures of ozone pollution in PRD and YRD during hot extremes, to consider the significant impacts of TC activities.

Extreme hot weathers are projected to be more frequent and intensified in the future under the continued global warming (P. Wang et al., 2019a). Moreover, it is projected that TCs and heatwave compound events are projected to significantly increase in their intensity and frequency over the Northwest Pacific, causing potentially enlarged population exposures for the southeastern coast of China (Wu et al. 2022). Therefore, the potential impacts of extreme hot weather and the TC-HDs on surface ozone over China warrants future efforts. BVOCs are important precursors of ozone, and their emissions are greatly influenced by weather conditions. As revealed by N. Wang et al. (2022), the TCs over Northwest Pacific could intensify the chemical interactions between anthropogenic and biogenic emissions, resulting in extreme ozone pollution over YRD and PRD regions. The responses of biogenic emissions during hot extremes accompanied by TCs deserve further investigation.

Data availability

The ground-level ozone concentrations are obtained from the high-resolution and high-quality ground-level daily maximum 8-hour average ozone (MDA8 O_3) data for China (ChinaHighO_3, https://doi.org/10.5281/zenodo.4400043). Daily maximum air temperature is provided by the National Meteorological Information Center of the China Meteorological Administration (CMA, http://data.cma.cn/en/). The best track dataset of tropical cyclones is also released by CMA (https://

tcdata.typhoon.org.cn/zjljsjj_sm.html). Meteorological conditions data are derived from the fifth generation of ECMWF reanalysis data (ERA5, https://cds.climate.copernicus.eu/). The GEOS-Chem model is available at http://acmg.seas.harvard.edu/geos/.

Author contributions

C. Qi performed the analyses and wrote the initial draft. P. Wang and Y. Yang conceived and supervised the study. H. Li performed the GEOS-Chem simulations. P. Wang reviewed and edited the initial draft. All the authors discussed the results and contributed to the final manuscript.

Competing interests

The authors declare that they have no competing interest.

Acknowledgements

This research was supported by the National Natural Science Foundation of China (grant 42293323, 42105166, and 41975159), the National Key Research and Development Program of China (grant 2020YFA0607803 and 2019YFA0606800), Jiangsu Science Fund for Distinguished Young Scholars (grant BK20211541, Y.Y.), and the Jiangsu Science Fund for Carbon Neutrality (grant BK20220031, H.L.).

References

Ainsworth, E.A., Yendrek, C.R., Sitch, S., Collins, W.J., Emberson, L.D.: The Effects of Tropospheric Ozone on Net Primary Productivity and Implications for Climate Change, Annu. Rev. Plant Biol., 63, 637–661, https://doi.org/10.1146/annurev-arplant-042110-103829, 2012.

Ashmore, M.R.: Assessing the future global impacts of ozone on vegetation, Plant Cell Environ., 28, 949–964, https://doi.org/10.1111/j.1365-3040.2005.01341.x, 2005.

Banta, R.M., Senff, C.J., Alvarez, R.J., Langford, A.O., Parrish, D.D., Trainer, M.K., Darby, L.S., Michael Hardesty, R., Lambeth, B., Andrew Neuman, J.: Dependence of daily peak O_3 concentrations near Houston, Texas on environmental factors: Wind speed, temperature, and boundary-layer depth, Atmos. Environ., 45, 162–173, https://doi.org/10.1016/j.atmosenv.2010.09.030, 2011.

Chen, L., Liao, H., Zhu, J., Li, K., Bai, Y., Yue, X., Yang, Y., Hu, J., Zhang, M.: Increases in ozone-related mortality in China over 2013–2030 attributed to historical ozone deterioration and future population aging, Sci. Total Environ., 858, 159972, https://doi.org/10.1016/j.scitotenv.2022.159972, 2023.

Dai, H., Huang, G., Wang, J., Zeng, H.: VAR-tree model based spatio-temporal characterization and prediction of O_3 concentration in China, Ecotoxicol. Environ. Saf., 257, 114960, https://doi.org/10.1016/j.ecoenv.2023.114960, 2023.

Ding, H., Kong, L., You, Y., Mao, J., Chen, W., Chen, D., ... & Wang, X.: Effects of tropical cyclones with different tracks on ozone pollution over the Pearl River Delta region, Atmos. Res., 286, 106680, https://doi.org/10.1016/j.atmosres.2023.106680, 2023

Feng, Z., Hu, E., Wang, X., Jiang, L., Liu, X.: Ground-level O_3 pollution and its impacts on food crops in China: A review, Environ. Pollut., 199, 42–48, https://doi.org/10.1016/j.envpol.2015.01.016, 2015.

Fu, Y., Liao, H.: Impacts of land use and land cover changes on biogenic emissions of volatile organic compounds in China from the late 1980s to the mid-2000s: implications for tropospheric ozone and secondary organic aerosol, Tellus B Chem. Phys. Meteorol., 66, 24987, https://doi.org/10.3402/tellusb.v66.24987, 2014.

Fu, Y., Liao, H., Yang, Y.: Interannual and Decadal Changes in Tropospheric Ozone in China and the Associated Chemistry-Climate Interactions: A Review, Adv. Atmospheric Sci., 36, 975–993, https://doi.org/10.1007/s00376-019-8216-9, 2019.

Gelaro, R., McCarty, W., Suárez, M. J., Todling, R., Molod, A., Takacs, L., Randles, C. A., Darmenov, A., Bosilovich, M. G., Reichle, R., Wargan, K., Coy, L., Cullather, R., Draper, C., Akella, S., Buchard, V., Conaty, A., Da Silva, A. M., Gu, W., … Zhao, B.: The Modern-Era Retrospective Analysis for Research and Applications, Version 2 (MERRA-2), J. Climate, 30, 5419–5454, https://doi.org/10.1175/JCLI-D-16-0758.1, 2017.

Gong, C., Liao, H.: A typical weather pattern for ozone pollution events in North China, Atmospheric Chem. Phys., 19, 13725–13740, https://doi.org/10.5194/acp-19-13725-2019, 2019.

Gori, A., Lin, N., Xi, D., & Emanuel, K.: Tropical cyclone climatology change greatly exacerbates US extreme rainfall–surge hazard, Nat. Clim. Chang., 12, 171–178, https://doi.org/10.1038/s41558-021-01272-7, 2022.

Gu, X., Wang, T., Li, C.: Elevated ozone decreases the multifunctionality of belowground ecosystems, Glob. Change Biol., 29, 890–908, https://doi.org/10.1111/gcb.16507, 2023.

Guenther, A.B., Jiang, X., Heald, C.L., Sakulyanontvittaya, T., Duhl, T., Emmons, L.K., Wang, X.: The Model of Emissions of Gases and Aerosols from Nature version 2.1 (MEGAN2.1): an extended and updated framework for modeling biogenic emissions, Geosci. Model Dev., 5, 1471–1492, https://doi.org/10.5194/gmd-5-1471-2012, 2012.

Han, W., Wang, Y., & Liu, L.: The relationship between pre-landfall intensity change and post-landfall weakening of tropical cyclones over China, Front. Earth Sci., 10, 1082181, https://doi.org/10.3389/feart.2022.1082181, 2022.

H. Hersbach, B. Bell, P. Berrisford, S. Hirahara, A. Horányi, J. Muñoz-Sabater, J. Nicolas, C. Peubey, R. Radu, D. Schepers, A. Simmons, C. Soci, S. Abdalla, X. Abellan, G. Balsamo, P. Bechtold, G. Biavati, J. Bidlot, M. Bonavita, G. de Chiara, P. Dahlgren, D. Dee, M. Diamantakis, R. Dragani, J. Flemming, R. Forbes, M. Fuentes, A. Geer, L. Haimberger, S. Healy, R. J. Hogan, E. Hólm, M. Janisková, S. Keeley, P. Laloyaux, P. Lopez, C. Lupu, G. Radnoti, P. de Rosnay, I. Rozum, F. Vamborg, S. Villaume, J. N. Thépaut,.: The ERA5 global reanalysis, Q. J. R. Meteorol. Soc., 146(730), 1999-2049, https://doi.org/10.1002/qj.3803, 2020.

Hoesly, R.M., Smith, S.J., Feng, L., Klimont, Z., Janssens-Maenhout, G., Pitkanen, T., Seibert, J.J., Vu, L., Andres, R.J., Bolt, R.M., Bond, T.C., Dawidowski, L., Kholod, N., Kurokawa, J., Li, M., Liu, L., Lu, Z., Moura, M.C.P., O'Rourke, P.R., Zhang, Q.: Historical (1750–2014) anthropogenic emissions of reactive gases and aerosols from the Community Emissions Data System (CEDS), Geosci. Model Dev., 11, 369–408, https://doi.org/10.5194/gmd-11-369-2018,

2018.

Huang, C., Chen, C. H., Li, L., Cheng, Z., Wang, H. L., Huang, H. Y., Streets, D. G., Wang, Y. J., Zhang, G. F., and Chen, Y. R.: Emission inventory of anthropogenic air pollutants and VOC species in the Yangtze River Delta region, China, Atmos. Chem. Phys., 11, 4105–4120, https://doi.org/10.5194/acp-11-4105-2011, 2011.

Huang, J., Pan, X., Guo, X., Li, G.: Health impact of China's Air Pollution Prevention and Control Action Plan: an analysis of national air quality monitoring and mortality data, Lancet Planet. Health, 2, e313–e323, https://doi.org/10.1016/S2542-5196(18)30141-4, 2018.

Jacob, D.J., Logan, J.A., Murti, P.P.: Effect of rising Asian emissions on surface ozone in the United States, Geophys. Res. Lett., 26, 2175–2178, https://doi.org/10.1029/1999GL900450, 1999.

Jammalamadaka, S.R., Lund, U.J.: The effect of wind direction on ozone levels: a case study, Environ. Ecol. Stat., 13, 287–298, https://doi.org/10.1007/s10651-004-0012-7, 2006.

Ji, X., Chen, G., Chen, J., Xu, L., Lin, Z., Zhang, K., Fan, X., Li, M., Zhang, F., Wang, H., Huang, Z., & Hong, Y.: Meteorological impacts on the unexpected ozone pollution in coastal cities of China during the unprecedented hot summer of 2022, Sci. Total Environ., 914, 170035, https://doi.org/10.1016/j.scitotenv.2024.170035, 2024.

Jiang, Z., Li, J., Lu, X., Gong, C., Zhang, L., Liao, H.: Impact of western Pacific subtropical high on ozone pollution over eastern China, Atmospheric Chem. Phys., 21, 2601–2613, https://doi.org/10.5194/acp-21-2601-2021, 2021.

Kavassalis, S.C., Murphy, J.G.: Understanding ozone-meteorology correlations: A role for dry deposition, Geophys. Res. Lett., 44, 2922–2931, https://doi.org/10.1002/2016GL071791, 2017.

Li, K., Jacob, D.J., Liao, H., Shen, L., Zhang, Q., Bates, K.H.: Anthropogenic drivers of 2013–2017 trends in summer surface ozone in China, Proc. Natl. Acad. Sci., 116, 422–427, https://doi.org/10.1073/pnas.1812168116, 2019.

Li, M., Yu, S., Chen, X., Li, Z., Zhang, Y., Wang, L., Liu, W., Li, P., Lichtfouse, E., Rosenfeld, D., and Seinfeld, J. H.: Large scale control of surface ozone by relative humidity observed during warm seasons in China, Environ. Chem. Lett., 19, 3981–3989, https://doi.org/10.1007/s10311-021-01265-0, 2021.

Lin, X., Yuan, Z., Yang, L., Luo, H., Li, W.: Impact of Extreme Meteorological Events on Ozone in the Pearl River Delta, China, Aerosol Air Qual. Res., 19, 1307–1324, https://doi.org/10.4209/aaqr.2019.01.0027, 2019.

Liu, H., Liu, S., Xue, B., Lv, Z., Meng, Z., Yang, X., Xue, T., Yu, Q., He, K.: Ground-level ozone pollution and its health impacts in China, Atmos. Environ., 173, 223–230, https://doi.org/10.1016/j.atmosenv.2017.11.014, 2018.

Lu, X., Yu, H., Ying, M., Zhao, B., Zhang, S., Lin, L., Bai, L., Wan, R.: Western North Pacific Tropical Cyclone Database Created by the China Meteorological Administration, Adv. Atmospheric Sci., 38, 690–699, https://doi.org/10.1007/s00376-020-0211-7, 2021.

Lu, X., Zhang, L., Chen, Y., Zhou, M., Zheng, B., Li, K., Liu, Y., Lin, J., Fu, T.-M., Zhang, Q.: Exploring 2016–2017 surface ozone pollution over China: source contributions and meteorological influences, Atmospheric Chem. Phys., 19, 8339–8361, https://doi.org/10.5194/acp-19-8339-2019, 2019.

Luo, M., & Lau, N.-C.: Heat Waves in Southern China: Synoptic Behavior, Long-Term Change, and

Urbanization Effects, J. Climate, 30(2), 703–720, https://doi.org/10.1175/JCLI-D-16-0269.1, 2017.

Ma, M., Gao, Y., Wang, Y., Zhang, S., Leung, L.R., Liu, C., Wang, S., Zhao, B., Chang, X., Su, H., Zhang, T., Sheng, L., Yao, X., Gao, H.: Substantial ozone enhancement over the North China Plain from increased biogenic emissions due to heat waves and land cover in summer 2017, Atmos Chem Phys., 19, 12195-12207, https://doi.org/10.5194/acp-19-12195-2019, 2019.

Matthews, T., Wilby, R.L., Murphy, C.: An emerging tropical cyclone–deadly heat compound hazard, Nat. Clim. Change, 9, 602–606, https://doi.org/10.1038/s41558-019-0525-6, 2019.

Meng, K., Zhao, T., Xu, X., Hu, Y., Zhao, Yang, Zhang, L., Pang, Y., Ma, X., Bai, Y., Zhao, Yuguang, Zhen, S.: Anomalous surface O_3 changes in North China Plain during the northwestward movement of a landing typhoon, Sci. Total Environ., 820, 153196, https://doi.org/10.1016/j.scitotenv.2022.153196, 2022.

Meng, X., Wang, W., Shi, S., Zhu, S., Wang, P., Chen, R., Xiao, Q., Xue, T., Geng, G., Zhang, Q., Kan, H., Zhang, H.: Evaluating the spatiotemporal ozone characteristics with high-resolution predictions in mainland China, 2013–2019, Environ. Pollut., 299, 118865, https://doi.org/10.1016/j.envpol.2022.118865, 2022.

Ni, Y., Yang, Y., Wang, H., Li, H., Li, M., Wang, P.: Contrasting changes in ozone during 2019–2021 between eastern China and the other regions of China, Sci. Total Environ., 908, 168272, http://dx.doi.org/10.2139/ssrn.4563723, 2024.

Ouyang, S., Deng, T., Liu, R., Chen, J., He, G., Leung, J.C.H., Wang, N., Liu, S.C.: Impact of a subtropical high and a typhoon on a severe ozone pollution episode in the Pearl River Delta,

China, Atmospheric Chem. Phys., 22(16), 10751-10767, https://doi.Org/10.5194/acp-22-10751-2022, 2022.

Pye, H.O.T., Liao, H., Wu, S., Mickley, L.J., Jacob, D.J., Henze, D.K., Seinfeld, J.H.: Effect of changes in climate and emissions on future sulfate-nitrate-ammonium aerosol levels in the United States, J. Geophys. Res. Atmospheres, 114, 2008JD010701, https://doi.org/10.1029/2008JD010701, 2009.

Qu, K., Wang, X., Yan, Y., Shen, J., Xiao, T., Dong, H., Zeng, L., Zhang, Y.: A comparative study to reveal the influence of typhoons on the transport, production and accumulation of O_3 in the Pearl River Delta, Atmospheric Chem. Phys., 21, 11593–11612, https://doi.org/10.5194/acp-21-11593-2021, 2021.

Sherwen, T., Schmidt, J.A., Evans, M.J., Carpenter, L.J., Großmann, K., Eastham, S.D., Jacob, D.J., Dix, B., Koenig, T.K., Sinreich, R., Ortega, I., Volkamer, R., Saiz-Lopez, A., Prados-Roman, C., Mahajan, A.S., Ordóñez, C.: Global impacts of tropospheric halogens (Cl, Br, I) on oxidants and composition in GEOS-Chem, Atmospheric Chem. Phys., 16, 12239–12271, https://doi.org/10.5194/acp-16-12239-2016, 2016.

Shu, L., Xie, M., Wang, T., Gao, D., Chen, P., Han, Y., Li, S., Zhuang, B., Li, M.: Integrated studies of a regional ozone pollution synthetically affected by subtropical high and typhoon system in the Yangtze River Delta region, China, Atmospheric Chem. Phys., 16, 15801–15819, https://doi.org/10.5194/acp-16-15801-2016, 2016.

Song, X., Hao, Y.: An assessment of O_3-related health risks and economic losses in typical regions of China, Front. Public Health, 11, 1194340, https://doi.org/10.3389/fpubh.2023.1194340,

2023.

Tuleya, R. E., Bender, M. A., and Kurihara, Y.: A Simulation Study of the Landfall of Tropical Cyclones, Mon. Wea. Rev., 112, 124–136, https://doi.org/10.1175/1520-0493(1984)112<0124:ASSOTL>2.0.CO;2, 1984.

Turner, M.C., Jerrett, M., Pope, C.A., Krewski, D., Gapstur, S.M., Diver, W.R., Beckerman, B.S., Marshall, J.D., Su, J., Crouse, D.L., Burnett, R.T.: Long-Term Ozone Exposure and Mortality in a Large Prospective Study, Am. J. Respir. Crit. Care Med, 193, 1134–1142, https://doi.org/10.1164/rccm.201508-1633OC, 2016.

Van Der Werf, G.R., Randerson, J.T., Giglio, L., Van Leeuwen, T.T., Chen, Y., Rogers, B.M., Mu, M., Van Marle, M.J.E., Morton, D.C., Collatz, G.J., Yokelson, R.J., Kasibhatla, P.S.: Global fire emissions estimates during 1997–2016, Earth Syst. Sci. Data, 9, 697–720, https://doi.org/10.5194/essd-9-697-2017, 2017.

Wang, N., Huang, X., Xu, J., Wang, T., Tan, Z., Ding, A.: Typhoon-boosted biogenic emission aggravates cross-regional ozone pollution in China, Sci. Adv., 8, eabl6166, https://doi.org/10.1126/sciadv.abl6166, 2022.

Wang, P., Hui, P., Xue, D., & Tang, J.: Future projection of heat waves over China under global warming within the CORDEX-EA-II project, Clim. Dynam., 53(1–2), 957–973, https://doi.org/10.1007/s00382-019-04621-7, 2019a.

Wang, P., Leung, L. R., Lu, J., Song, F., & Tang, J.: Extreme wet-bulb temperatures in China: The significant role of moisture, J. Geophys. Res.: Atmos., 124(22), 11944–11960, https://doi.org/10.1029/2019JD031477, 2019b.

644 Wang, P., Tang, J., Wang, S., Dong, X., & Fang, J.: Regional heatwaves in china: a cluster analysis,
645 Clim. Dynam., 50, 1901–1917, https://doi.org/10.1007/s00382-017-3728-4, 2018.
646 Wang, P., Yang, Y., Li, H., Chen, L., Dang, R., Xue, D., Li, B., Tang, J., Leung, L.R., Liao, H.: North
647 China Plain as a hot spot of ozone pollution exacerbated by extreme high temperatures,
648 Atmospheric Chem. Phys., 22, 4705–4719, https://doi.org/10.5194/acp-22-4705-2022, 2022.
649 Wang, P., Yang, Y., Xue, D., Qu, Y., Tang, J., Leung, L.R., Liao, H.: Increasing Compound Hazards
650 of Tropical Cyclones and Heatwaves over Southeastern Coast of China under Climate Warming,
651 J. Clim., 36, 2243–2257, https://doi.org/10.1175/JCLI-D-22-0279.1, 2023.
652 Wang, T., Xue, L., Brimblecombe, P., Lam, Y.F., Li, L., Zhang, L.: Ozone pollution in China: A
653 review of concentrations, meteorological influences, chemical precursors, and effects, Sci.
654 Total Environ., 575, 1582–1596, https://doi.org/10.1016/j.scitotenv.2016.10.081, 2017.
655 Wang, T., Zhong, Z., Sun, Y., Wang, J.: Impacts of tropical cyclones on the meridional movement
656 of the western Pacific subtropical high, Atmospheric Sci. Lett., 20, e893,
657 https://doi.org/10.1002/asl.893, 2019.
658 Wang, W., Zhou, W., Li, X., Wang, X., Wang, D.: Synoptic-scale characteristics and atmospheric
659 controls of summer heat waves in China, Clim. Dynam., 46, 2923–2941,
660 https://doi.org/10.1007/s00382-015-2741-8, 2016.
661 Wang, X., Chen, F., Wu, Z., Zhang, M., Tewari, M., Guenther, A., & Wiedinmyer, C.: Impacts of
662 weather conditions modified by urban expansion on surface ozone: Comparison between the
663 Pearl River Delta and Yangtze River Delta regions, Adv. Atmos. Sci., 26, 962–972,
664 https://doi.org/10.1007/s00376-009-8001-2, 2009.

Wang, Z., Hu, B., Zhang, C., Atkinson, P.M., Wang, Z., Xu, K., Chang, J., Fang, X., Jiang, Y., Shi, Z.: How the Air Clean Plan and carbon mitigation measures co-benefited China in $PM_{2.5}$ reduction and health from 2014 to 2020, Environ. Int., 169, 107510 https://doi.org/10.1016/j.envint.2022.107510, 2022.

Wei, J., Li, Z., Li, K., Dickerson, R.R., Pinker, R.T., Wang, J., Liu, X., Sun, L., Xue, W., Cribb, M.: Full-coverage mapping and spatiotemporal variations of ground-level ozone (O_3) pollution from 2013 to 2020 across China, Remote Sens. Environ., 270, 112775, https://doi.org/10.1016/j.rse.2021.112775, 2022.

Wei, X., Lam, K. S., Cao, C., Li, H., & He, J.: Dynamics of the Typhoon Haitang Related High Ozone Episode over Hong Kong, Adv. Atmospheric Sci., 6089154, https://doi.org/10.1155/2016/6089154, 2016.

Wu, J., Chen, Y., Liao, Z., Gao, X., Zhai, P., & Hu, Y.: Increasing risk from landfalling tropical cyclone-heatwave compound events to coastal and inland China, Environ. Res. Lett., 17(10), 105007, https://doi.org/10.1088/1748-9326/ac9747, 2022.

Xiao, Y.F., Duan, Z.D., Xiao, Y.Q., Ou, J.P., Chang, L., Li, Q.S.: Typhoon wind hazard analysis for southeast China coastal regions, Struct. Saf., 33, 286–295, https://doi.org/10.1016/j.strusafe.2011.04.003, 2011.

Yang, Y., Li, M., Wang, H., Li, H., Wang, P., Li, K., Gao, M., Liao, H.: ENSO modulation of summertime tropospheric ozone over China, Environ. Res. Lett., 17, 034020, https://doi.org/10.1088/1748-9326/ac54cd, 2022.

Yang, Y., Liao, H., Li, J.: Impacts of the East Asian summer monsoon on interannual variations of

summertime surface-layer ozone concentrations over China, Atmospheric Chem. Phys., 14, 6867–6879, https://doi.org/10.5194/acp-14-6867-2014, 2014.

Yin, Z., Cao, B., Wang, H.: Dominant patterns of summer ozone pollution in eastern China and associated atmospheric circulations, Atmospheric Chem. Phys., 19, 13933–13943, https://doi.org/10.5194/acp-19-13933-2019, 2019.

Ying, M., Zhang, W., Yu, H., Lu, X., Feng, J., Fan, Y., Zhu, Y., Chen, D.: An Overview of the China Meteorological Administration Tropical Cyclone Database, J. Atmospheric Ocean. Technol., 31, 287–301, https://doi.org/10.1175/JTECH-D-12-00119.1, 2014.

Zhan, C., & Xie, M.: Exploring the link between ozone pollution and stratospheric intrusion under the influence of tropical cyclone Ampil, Sci. Total Environ., 828, 154261, https://doi.org/10.1016/j.scitotenv.2022.154261, 2022.

Zhan, C., Xie, M., Huang, C., Liu, J., Wang, T., Xu, M., Ma, C., Yu, J., Jiao, Y., Li, M., Li, S., Zhuang, B., Zhao, M., & Nie, D.: Ozone affected by a succession of four landfall typhoons in the Yangtze River Delta, China: Major processes and health impacts, Atmospheric Chem. Phys., 20(22), 13781–13799, https://doi.org/10.5194/acp-20-13781-2020, 2020.

Zhang, J., Gao, Y., Luo, K., Leung, L.R., Zhang, Y., Wang, K., Fan, J.: Impacts of compound extreme weather events on ozone in the present and future, Atmospheric Chem. Phys., 18, 9861–9877, https://doi.org/10.5194/acp-18-9861-2018, 2018.

Zhang, M., Yang, Y., Zhan, C., Zong, L., Gul, C., & Wang, M.: Tropical cyclone-related heatwave episodes in the Greater Bay Area, China: Synoptic patterns and urban-rural disparities. Weather and Climate Extremes, 44, 100656. https://doi.org/10.1016/j.wace.2024.100656, 2024.

Zhang, Y., Dai, J., Li, Q., Chen, T., Mu, J., Brasseur, G., Wang, T., Xue, L.: Biogenic volatile organic compounds enhance ozone production and complicate control efforts: Insights from long-term observations in Hong Kong, Atmos. Environ., 309, 119917, https://doi.org/10.1016/j.atmosenv.2023.119917, 2023.

Zhou, Y., Yang, Y., Wang, H., Wang, J., Li, M., Li, H., Wang, P., Zhu, J., Li, K., Liao, H.: Summer ozone pollution in China affected by the intensity of Asian monsoon systems, Sci. Total Environ., 849, 157785, https://doi.org/10.1016/j.scitotenv.2022.157785, 2022.

715 **Table 1.** Observed and simulated averaged surface MDA8 ozone (μg/m^3) in the Yangtze River Delta
716 (YRD, 118-122° E, 30-33° N) and the Pearl River Delta (PRD, 110-115.5° E, 21.5-24° N) during
717 TC-HDs and AHDs, as well as their differences (TC-HDs minus AHDs).

	YRD		**PRD**	
	Observed	Simulated	Observed	Simulated
TC-HDs	134.71	177.17	97.93	123.91
AHDs	147.92	199.11	91.13	116.91
Differences	−13.21	−21.94	6.8	7

718

719 **Table 2.** Contributions of difference processes for the anomalous ozone mass (Gg O_3/day) from
720 surface to 500 hPa for TC-HDs and AHDs relative to the summer climatology and their difference
721 (TC-HDs minus AHDs) for YRD.

	Net chemical production	Vertical advection	Horizontal advection	Mixing
TC-HDs	1.70	0.03	−2.18	0.004
AHDs	0.46	−0.04	−1.03	−0.12
Differences	1.24	0.07	−1.15	0.12

722

723

724

725 **Table 3.** Contributions of difference processes for the anomalous ozone mass (Gg O_3/day) from
726 surface to 500 hPa for TC-HDs and AHDs relative to the summer climatology and their difference
727 (TC-HDs minus AHDs) for PRD.

	Net chemical production	Vertical advection	Horizontal advection	Mixing
TC-HDs	0.21	−0.13	0.97	−0.002
AHDs	0.06	0.09	−0.84	−0.05
Differences	0.15	−0.22	1.81	0.05

728
729

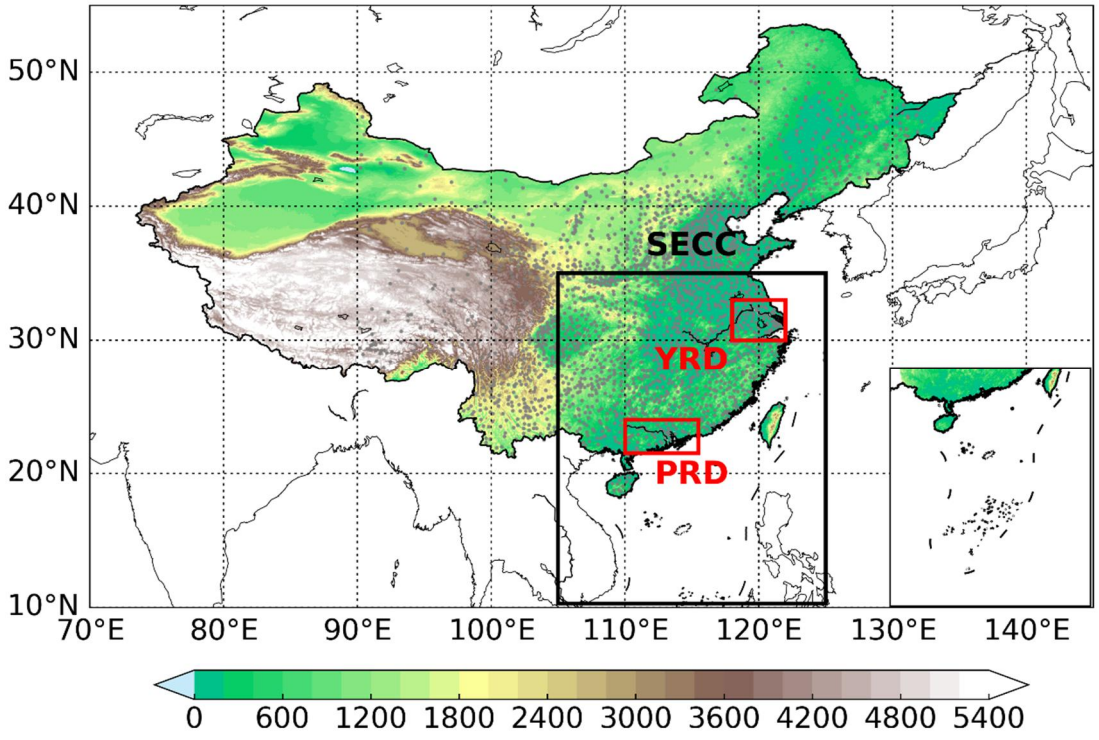

730

731 **Figure 1.** Topographic map of China with SECC (black box) and megacity clusters YRD and PRD

732 outlined (red boxes). Gray points represent the temperature observation stations.

733

734

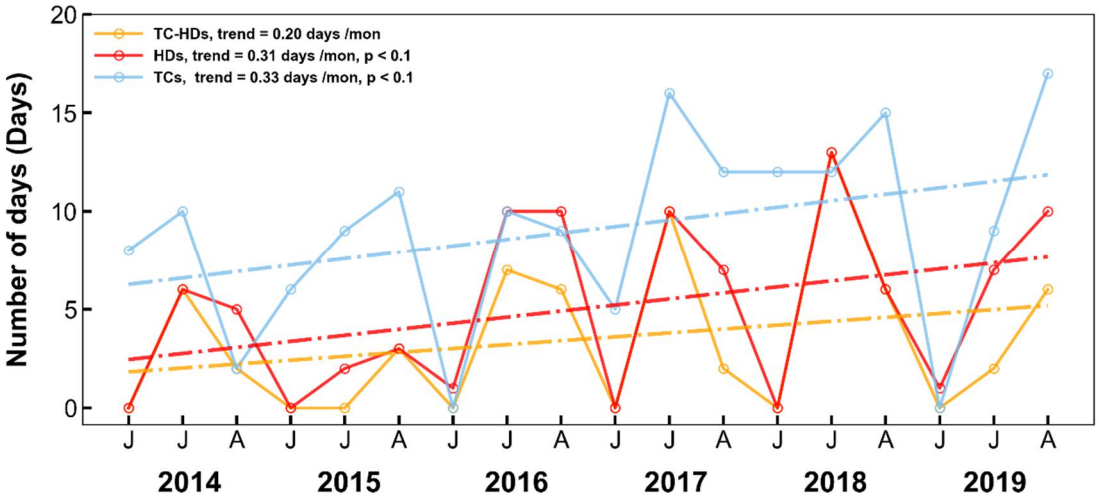

735

736 **Figure 2.** Monthly variations of the number of days of TC-HDs, total HDs, and total TCs during the

737 summer season (June, July and August) from 2014-2019.

738

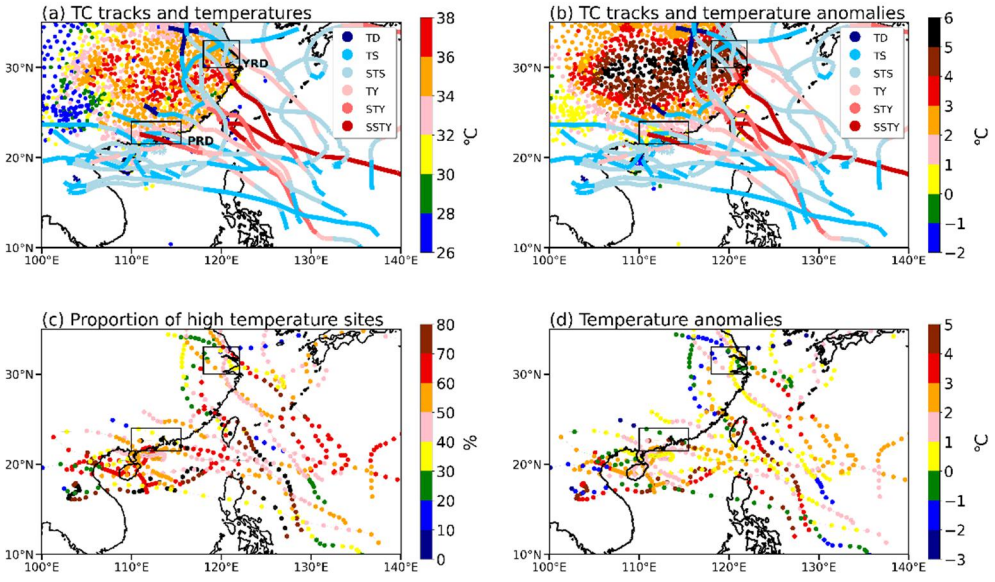

739

740 **Figure 3.** (a) The distribution of average Tmax (dots) and TC tracks during TC-HDs. (b) The Area

741 average of Tmax anomalies during TC-HDs period relative to the summer climatology (June to

742 August of 2014-2019), along with the TC tracks categorized by different intensities. (c) The

743 proportion of high-temperature sites (Tmax $\geqslant$ 35℃) over land region of SECC along with the

744 movements of the TCs. The proportion of high-temperature sites refers to the percentage of high-

745 temperature sites within all stations in the SECC region. (d) The average of Tmax anomalies for all

746 observational sites within SECC relative to the summer climatology, along with the movements of

747 TCs. YRD and PRD regions are outlined in black boxes in each panel.

748

749 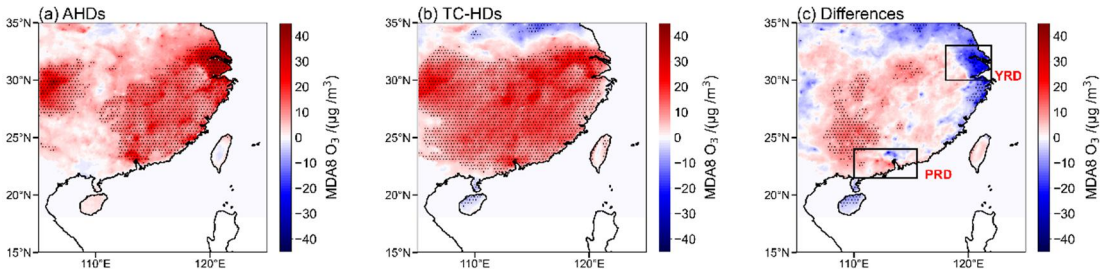

750 **Figure 4.** The spatial distribution of surface MDA8 ozone concentration anomalies during the
751 periods of (a) AHDs, (b) TC-HDs relative to the summertime climatology, as well as (c) their
752 differences (TC-HDs minus AHDs). Stippling regions indicate ozone anomalies that are
753 significantly difference from zero at the 95% confidence level. YRD and PRD regions are outlined
754 in black boxes in panel c.
755

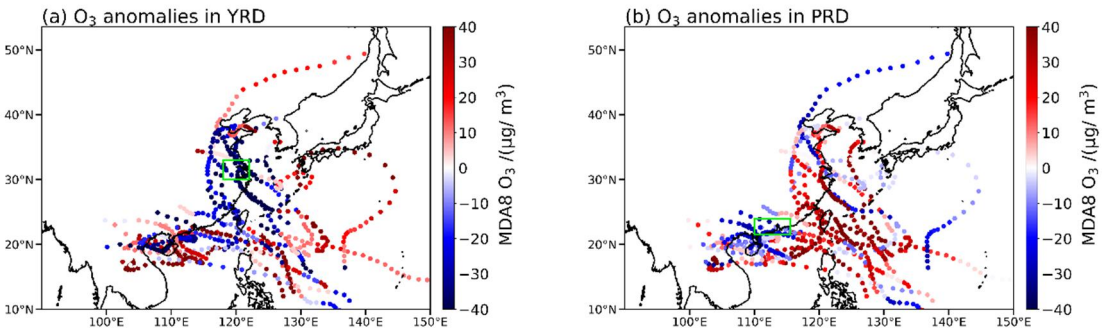

Figure 5. The average anomalies of surface MDA8 ozone concentrations over land regions of SECC along with the movements of TCs associated with TC-HDs for (a) YRD and (b) PRD regions. YRD (a) and PRD (b) regions are outlined in green boxes in panel (a) or (b).

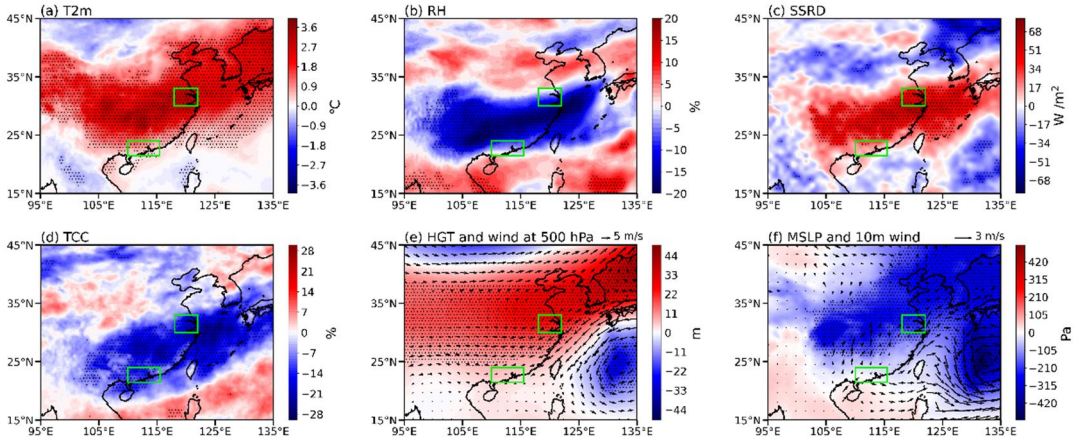

761

762 **Figure 6.** The spatial distribution for the composites anomalies of (a) air temperature at 2m (T2m),

763 (b) relative humidity (RH), (c) surface solar radiation downwards (SSRD), (d) total cloud cover

764 (TCC), (e) geopotential height (HGT) and winds at 500hPa, and (f) mean surface level pressure

765 (MSLP) and 10-meter winds during AHDs relative to the summer climatology. Stippling indicates

766 statistically significant anomalies above 95% confidence level. YRD and PRD regions are outlined

767 in green boxes in each panel.

768

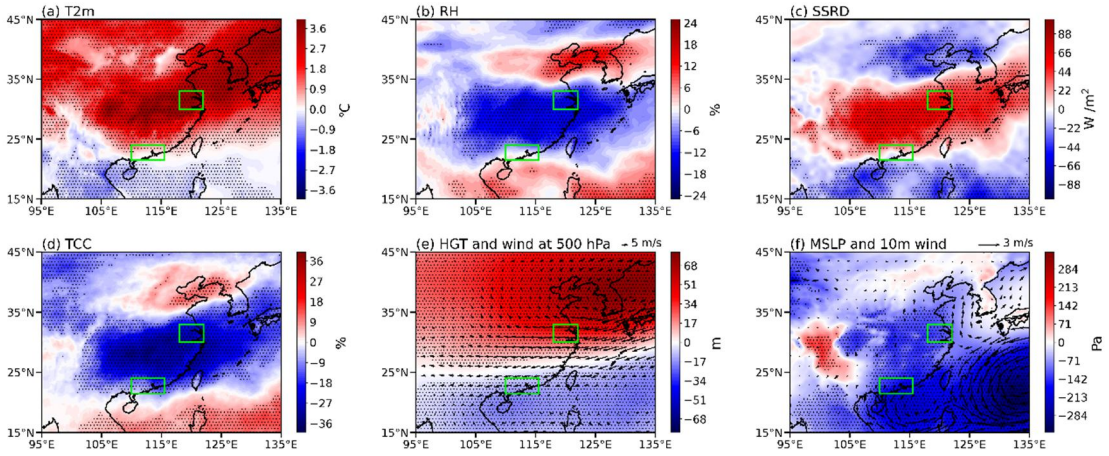

769

770 **Figure 7.** Same as in Figure 6, but for the anomalous meteorological conditions during TC-HDs.

771

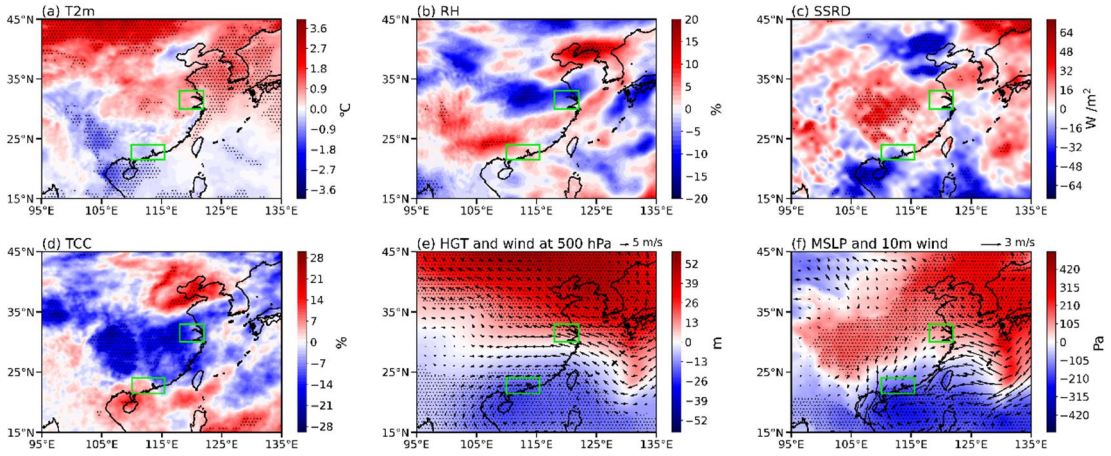

772

773 **Figure 8.** Same as in Figure 6, but for the differences between TC-HDs and AHDs (TC-HDs minus

774 AHDs).

775

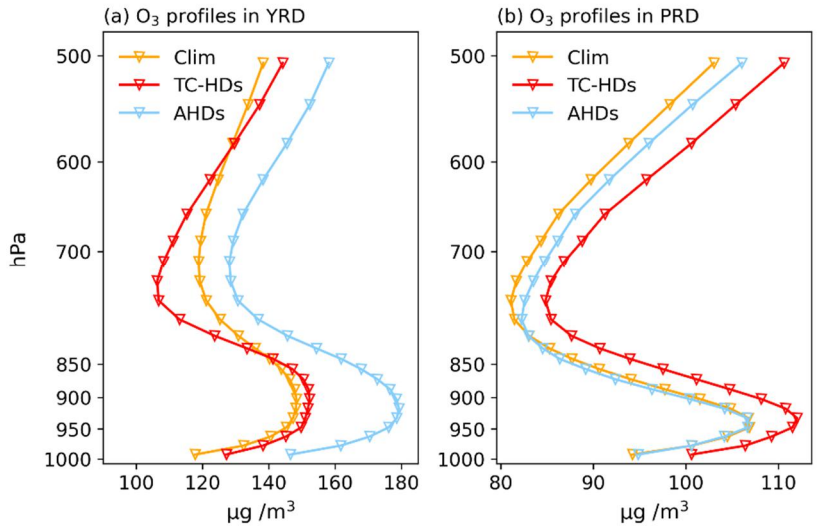

776

777 **Figure 9.** Vertical profiles of simulated daily ozone concentrations (μg/m^3) averaged over land

778 regions of SECC for TC-HDs, AHDs and for the summertime climatology (Clim) during 2014-2019

779 for (a) YRD and (b) PRD.

780

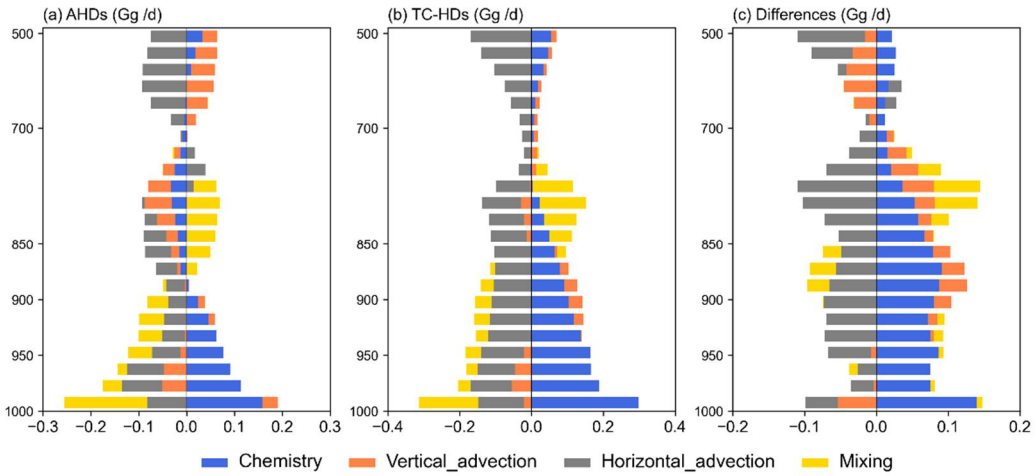

781

782 **Figure 10.** Vertical profiles of net changes in ozone mass (Gg O_3/day) anomalies averaged for YRD

783 for each process during (a) AHDs, (b) TC-HDs relative to summertime climatology, and their

784 differences (TC-HDs minus AHDs).

785

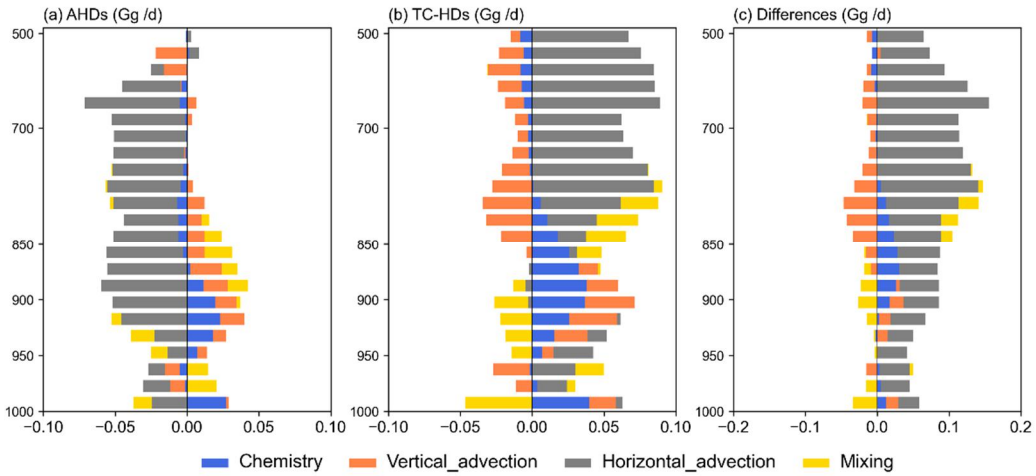

786

787 **Figure 11.** Same as in Figure 10, but for the vertical profiles of net changes in ozone mass (Gg

788 O_3/day) anomalies averaged for PRD for each process.